IJIRCCE

e-ISSN: 2320-9801 | p-ISSN: 2320-9798

INTERNATIONAL JOURNAL OF INNOVATIVE RESEARCH

IN COMPUTER & COMMUNICATION ENGINEERING

Volume 12, Issue 4, April 2024

INTERNATIONAL STANDARD SERIAL NUMBER INDIA

Impact Factor: 8.379

International Journal of Innovative Research in Computer and Communication Engineering

| e-ISSN: 2320-9801, p-ISSN: 2320-9798| www.ijircce.com | |Impact Factor: 8.379 | Monthly Peer Reviewed & Referred Journal |

|| Volume 12, Issue 4, April 2024 ||

| DOI: 10.15680/IJIRCCE.2024.1204286 |

Cost-Effective Segmentation of Lung Veins & Rapid Reformation Using Supervised Learning

Mr. S. R. Sridhar, Yokeshwar V, Pravinkumar D, Pradeep S

Assistant Professor, Department of CSE, Muthayammal Engineering College (Autonomous), Rasipuram, Tamil Nadu, India

Department of CSE, Muthayammal Engineering College (Autonomous), Rasipuram, Tamil Nadu, India

Department of CSE, Muthayammal Engineering College (Autonomous), Rasipuram, Tamil Nadu, India

Department of CSE, Muthayammal Engineering College (Autonomous), Rasipuram, Tamil Nadu, India

ABSTRACT: A new software module for coronary CTA analysis has been presented. The interactive processing is accelerated by non-supervised coronary artery extraction running in the background before the user opens the dataset. In this preliminary experiment, both accuracy and efficiency seem acceptable. Further work will include improved segmentation of calcifications and CPU time management of the automatic processing thread. However, this also results in increasing amounts of image data generated by each examination. The typical number of images has increased from one optimal phase of around 100 slices to multiple useful phases of 300-500 slices. Finding an efficient method to extract useful information from this amount of data has become a focus of medical image processing researchers.

KEYWORDS: Predictive Modeling, Artificial Intelligence, Medicine; Computational Models, Forecasting, Future

I. INTRODUCTION

Medical imaging is one of the most commonly used techniques in health-care for assisting with diagnosis and treatment of patients[1]. Medical imaging is unique in the diagnostic armamentarium because it is generally non-invasive, natively digital, and highly versatile in enabling detection, monitoring, and even prediction of disease. There are a variety of means that are used in creating images of the human body such as ultrasound, magnetic resonance, computer tomography, X-rays, etc. [2]. Advances in medical imaging have greatly improved the accuracy of screening for these diseases at earlier stages. However, 3D medical images such as computer tomography (CT) and magnetic resonance imaging (MRI) remain relatively expensive and their availability is limited in most parts of the world.

The use of X-rays, on the other hand, is considered the most popular and affordable medical imaging technique worldwide. X-ray imaging is crucial in a variety of medical settings from community clinics to tertiary referral center. Chest X-Rays are widely used to detect infections, such as pneumonia, as well as other relevant pathologies such as lung nodules or pulmonary edema. Due to the effectiveness of chest radiographs, millions of CXRs are generated annually as an initial diagnostic tool, which accounts for about one-third of all medical imaging procedures [3]. However, the use of CXRs for diagnosis is non-trivial and requires a high level of skill, experience, and concentration from the radiologist [4]. It can be a considerable or altogether infeasible diagnostic workload to examine millions of CXRs, especially considering that there is a shortage of radiologists worldwide [5]. According to the Association of American Medical Colleges, it is estimated that the United States could experience such a shortfall of radiologists by 2033 [6].

International Journal of Innovative Research in Computer and Communication Engineering

| e-ISSN: 2320-9801, p-ISSN: 2320-9798| www.ijircce.com | |Impact Factor: 8.379 | Monthly Peer Reviewed & Referred Journal |

|| Volume 12, Issue 4, April 2024 ||

| DOI: 10.15680/IJIRCCE.2024.1204286 |

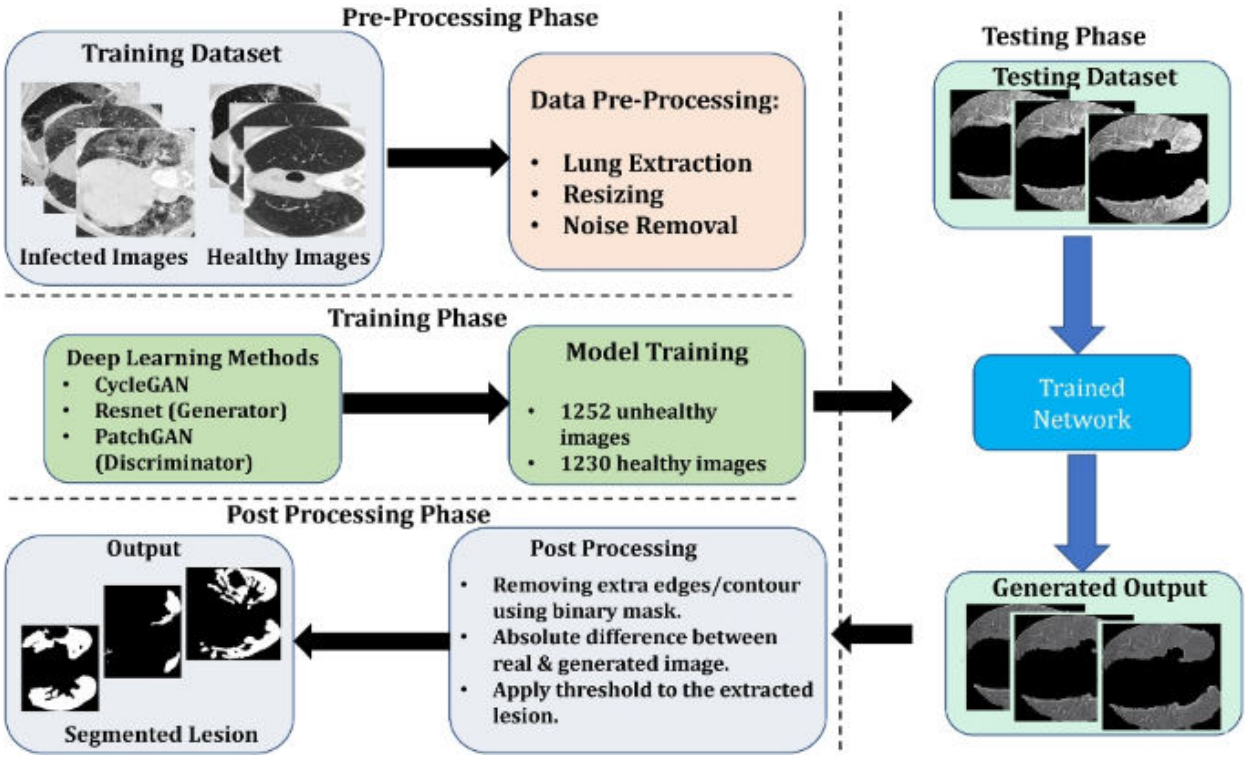

Fig 1: Lesion segmentation in lung CT scans

This necessitates the demand for automated medical diagnostics tools to aid medical professionals. Given this fact, researchers continue to explore the use of different techniques and algorithms to develop automated and computer-aided methods to assist radiologists in reading chest radiographs [7, 8]. Such an attempt was pioneered by Lodwick et. al. [9] through the development of a computer-aided detection (CAD) system. Later, many efforts have been made to improve the accuracy of the CAD system and commercialize it for clinical applications, including CAD4 TB, Riverain, and Delft imaging systems [10, 11]. However, due to the complex nature of CXRs, automatic and accurate detection of diseases remains unresolved in most of the existing CAD systems. CAD systems are mainly divided into four steps: image processing, region of interest (ROI) extraction, ROI features detection, and diseases classification according to the features. It is worth mentioning that classical approaches have involved manual feature extraction within this workflow. Recent development of machine learning algorithms, accumulation of voluminous medical images, and computational power open up new opportunities for building modern CAD systems [12]. For example, in reading chest radiographs, the task of extracting ROIs is now largely replaced by lung segmentation and, once a relevant lung region is segmented, shape irregularities, size, and other abnormalities of the lungs can be analyzed to identify clinical conditions such as pleural effusion, emphysema, and pneumothorax [13]. Hence, lung segmentation is one of the crucial steps in CAD-based disease detection using CXRs and ongoing success in effective segmentation will increase the scale and utility of CAD.

II. RELATED WORKS

Lung segmentation is a preliminary and fundamental task in computer-aided diagnostics systems. In light of this fact, the scientific community has shown great interest in this field and contributed to improving the lung segmentation in CXR. In this section, we reviewed some of the most relevant works in this research area. Based on current literature, lung segmentation techniques can be divided into two broad approaches i.e., 1) the classical approach using conventional image processing techniques and 2) convolutional neural networks (CNNs) based approaches.

Saad et. al. [14] proposed a method for segmenting lung regions in CXR images using the canny edge filter and image morphology. Before deploying the edge filter, the method utilized the Euler number to improve the accuracy of lung edge detection. An implementation of this method produced segmentation results with an overall Dice score of 0.809 on the JSRT dataset. Another edge-based method was proposed by Xu et. al. in [15], where the global edge and region force (ERF) field-based active shape model (ASM) called ERF-ASM is used to segment the lung field in CXR. This

| e-ISSN: 2320-9801, p-ISSN: 2320-9798| www.ijircce.com | |Impact Factor: 8.379 | Monthly Peer Reviewed & Referred Journal |

|| Volume 12, Issue 4, April 2024 ||

| DOI: 10.15680/IJIRCCE.2024.1204286 |

method applied the principal component analysis (PCA) to learn the shape of the lung fields in advance, which is then applied to regularize the ERF-based segmentation and obtained the overall accuracy and sensitivity of 0.955 and 0.912, respectively on the JSRT dataset. Ahmad et. al. [16] presented another method based on an oriented Gaussian derivatives filter with seven orientations, combined with Fuzzy C-Means (FCM) clustering and thresholding to refine the lung region. The performance of this method greatly depends on the initial selection of the number of orientations and thresholds. This method reached a Jaccard index value of 0.870 and an accuracy of 0958 on the JSRT dataset. Due to the effectiveness of accurate thresholding and Gaussian derivatives, Kiran et. al.[17] presented a six-step lung segmentation methodology based on Sauvola thresholding and Gaussian derivative (ST-GD). This method achieved an accuracy of 0.9457 on the JSRT dataset and 0.9075 on the MC dataset.

Besides its more obvious role in data augmentation, generative adversarial networks (GANs) are also being utilized in classification and segmentation applications. Thus, a research framework has recently been developed by Munawar et. al. in [26]. Given an input CXR, a GAN network is trained to generate a mask and, later, a discriminator distinguishes between ground truth and the generated mask. The authors trained four different discriminators, D1, D2, D3, and D4, among which D2 obtained the highest DC value of 0.9780 on the MC dataset. In another work, Chen et. al. [27] proposed semantic-aware GANs for unsupervised domain adaptation called SeUDA. The distinct feature of this method is that it detaches the segmentation deep neural network (DNN) from the domain adaptation process and does not require any labels from the test set. The SeUDA framework conducts image-to-image transformation to generate a source-like image which is directly forwarded to the DNN. This framework achieved a Dice value of 0.9559 and 0.9342 for the right and left lung respectively on JSRT dataset.

III. METHODOLOGY

This section provides all relevant details and a step-by-step explanation of our lung segmentation methodology. The proposed framework consists of five major steps: image pre-processing and patch extraction, CNN-based classifier, an adapted U-Net-based patch segmentation, generation of an initial segmentation, and post-processing to obtain the final segmentation as shown in Figure 1. The details of each of these steps are explained in the following subsections.

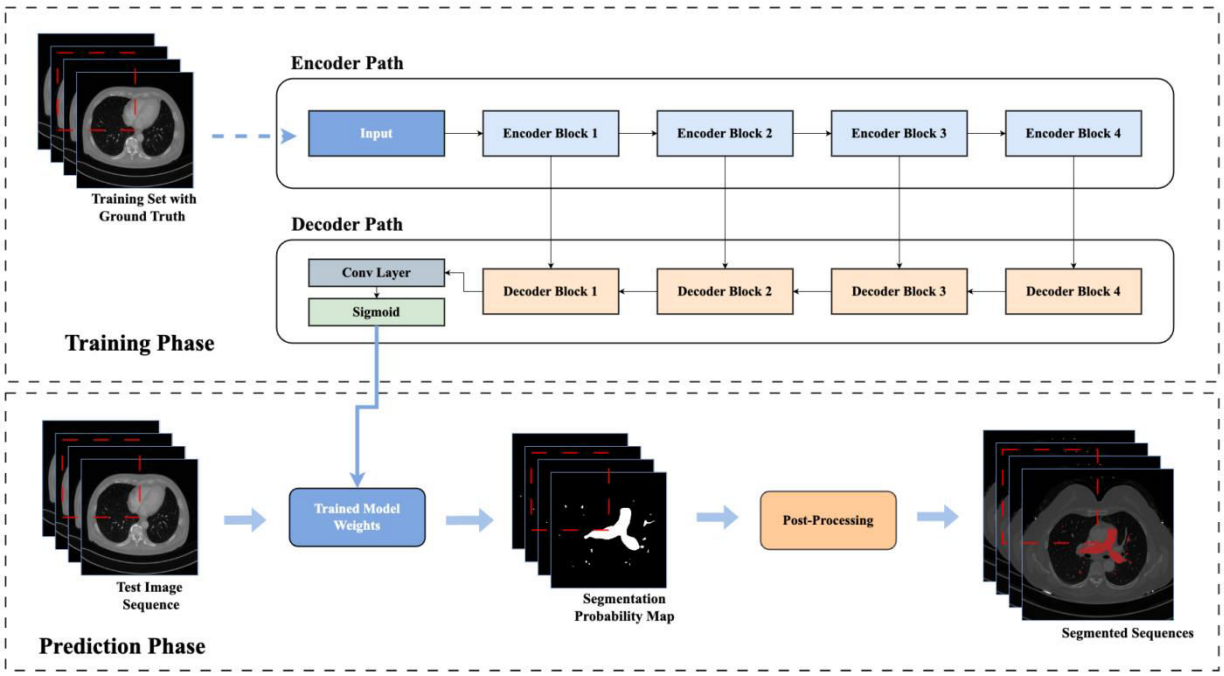

Fig 2: Segmentation Of Lung Veins

The datasets used in this paper have been collected from the Tuberculosis Control Program of the Department of Health and Human Services of Montgomery County (MC), Maryland, USA (https://lhncbc.nlm.nih.gov/publication/pub9931) and Japanese Society of Radiological Technology which is commonly known as the JSRT database (http://db.jsrt.or.jp/eng.php). The 7 MC database and the JSRT database are publicly available and commonly used in

| e-ISSN: 2320-9801, p-ISSN: 2320-9798| www.ijircce.com | |Impact Factor: 8.379 | Monthly Peer Reviewed & Referred Journal |

|| Volume 12, Issue 4, April 2024 ||

| DOI: 10.15680/IJIRCCE.2024.1204286 |

various areas of digital imaging including image processing, image enhancement, computer-aided diagnosis, and lung region segmentation. The MC dataset contains 138 posterior-anterior X-rays, of which 80 X-rays are normal and 58 are abnormal with a manifestation of tuberculosis. The X-rays are available in two different sizes either 4020 × 4892 or 4892 × 4020 pixels. The JSRT dataset contains 247 images, among which 154 X-rays have lung nodules (100 malignant cases, 54 benign cases) and 93 X-rays are normal without any lung nodules (non-nodules). The image size is 2048 × 2048. Both the MC and JSRT dataset come with corresponding ground truth masks which make them convenient for supervised learning. We also used another proprietary dataset, which is provided by the University of Texas Medical Branch (UTMB).

As mentioned in the previous section, we combined X-rays from three different sources which come in different sizes and formats. First, we downscaled all images to 512 × 512 to reduce the computational cost of model training. While downscaling the images, the MC X-rays were first placed in the center of the 4892 × 4892 background images and later downscaled to 512 × 512. Notice that, since the MC dataset has X-ray images in two different sizes, direct resizing could distort image proportion. For JSRT and UTMB datasets, we directly resized the images since the original images have identical width and height. After resizing the images, the pixel values of the X-ray images are normalized, i.e., the pixel intensity is mapped into the range between 0 and 1, where 0 is black and 1 is white. The values between 0 and 1 represent the shades of gray. This is particularly important when combining datasets from separate institutions as the different datasets may have different ranges of pixel values. Moreover, image normalization or enhancement has a positive effect on the outcome of the deep learning model [30-33].

IV. RESULT ANALYSIS

At this stage, we have obtained a precise contour along with segmentation. However, it can still contain noise and inaccuracies, which are mainly due to the prediction error of an individual Xray patch from either the CNN model or the U-Net model. For example, a background patch or a portion thereof could be erroneously segmented as lung region, as highlighted in Figure 4 in orange. Alternatively, a lung region could be segmented as a background patch, as marked in Figure 4 in red and yellow. These errors are sometimes inevitable as some of the background and lung region patches are difficult to distinguish when a whole X-ray image is divided into small patches. This problem is addressed by utilizing several image morphological operations such as erosion, dilation, closing, and connected component labeling algorithm in the post-processing step. The reader is referred to ref. [43-45] for a more detailed description of morphological operations. The erosion operation is used to erode tiny noises and separate noises weakly connected with the lung contour.

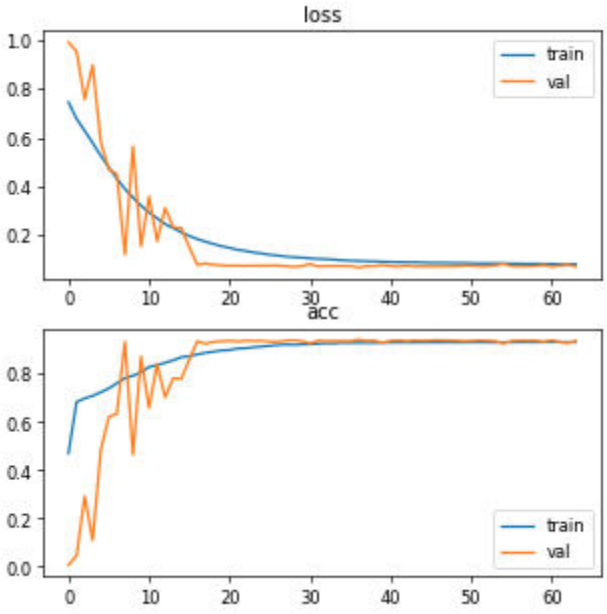

Fig 3: Result analysis

| e-ISSN: 2320-9801, p-ISSN: 2320-9798| www.ijircce.com | |Impact Factor: 8.379 | Monthly Peer Reviewed & Referred Journal |

|| Volume 12, Issue 4, April 2024 ||

| DOI: 10.15680/IJIRCCE.2024.1204286 |

However, deploying the erosion operation shrinks the lung region, which is recovered by the dilation operation. The connected component algorithm is used to identify the size of the remaining scattered noises after deploying the erosion operation. Subsequently, noises of size less than 3,000 pixels are. The necessity of this step is quite obvious as a good segmentation should only contain the two large lung parts. The region filling algorithm is utilized to fill in any internal gap laying inside the lung region. The structuring elements used in the above morphological operation are set as a square of size 11 × 11, an ellipse of size 9 × 9, and an ellipse of size 23 × 23 for the erosion, dilation, and closing operation, respectively. We choose the kernel size based on several experiments with the segmented masks.

V. CONCLUSIONS

In this work, we proposed a fully automated deep learning framework to increase the accuracy of lung segmentation in CXRs. The framework is divided into three major stages. First, we extract small patches from the original CXR images. Second, the extracted patches are classified and segmented by deploying an ensemble of a CNN model and an adapted U-Net model. Later, the patches are merged back to obtain two pre-segmentation masks. Subsequently, the presegmentation masks are combined together using the binary OR operation, which is later postprocessed to generate the final segmented mask. The novelty of this framework is that the two concurrently employed parallel deep learning models complement each other by capturing missing pixels in two pre-segmentation masks. Thus, merging the pre-segmented masks helps to increase the overall segmentation accuracy, especially for the CXRs from patients affected by pulmonary disease. It is worth mentioning that, this framework can efficiently utilize small datasets for training the CNNs.

REFERENCES

[1] W. R. Hendee et al., "Addressing overutilization in medical imaging," Radiology, vol. 257, no. 1, pp. 240-245, 2010.
[2] R. S. Mackay, "Medical images and displays. Comparisons of nuclear magnetic resonance, ultrasound, X-rays, and other modalities," United States, 1984.
[3] B. Van Ginneken, B. T. H. Romeny, and M. A. Viergever, "Computer-aided diagnosis in chest radiography: a survey," IEEE Transactions on Medical Imaging, vol. 20, no. 12, pp. 1228-1241, 2001. 24
[4] L. G. Quekel, A. G. Kessels, R. Goei, and J. M. van Engelshoven, "Miss rate of lung cancer on the chest radiograph in clinical practice," Chest, vol. 115, no. 3, pp. 720-724, 1999.
[5] G. Torres-Mejía et al., "Radiographers supporting radiologists in the interpretation of screening mammography: a viable strategy to meet the shortage in the number of radiologists," BMC Cancer, vol. 15, no. 1, pp. 1-12, 2015.
[6] W. J. Palmer. "Physician Specialty Shortage - Including Radiologist - Continue to Climb." Diagnostic Imaging. Available at: https://www.diagnosticimaging.com/view/theimpact-of-price-transparency-in-radiology (accessed March 1, 2021).
[7] S. Katsuragawa and K. Doi, "Computer-aided diagnosis in chest radiography," Computerized Medical Imaging and Graphics, vol. 31, no. 4-5, pp. 212-223, 2007.
[8] N. Mahomed et al., "Computer-aided diagnosis for World Health Organization-defined chest radiograph primary-endpoint pneumonia in children," Pediatric radiology, vol. 50, no. 4, pp. 482-491, 2020.
[9] G. S. Lodwick, T. E. Keats, and J. P. Dorst, "The coding of roentgen images for computer analysis as applied to lung cancer," Radiology, vol. 81, no. 2, pp. 185-200, 1963.
[10] A. Zakirov, R. Kuleev, A. Timoshenko, and A. Vladimirov, "Advanced approaches to computer-aided detection of thoracic diseases on chest X-rays," Appl Math Sci, vol. 9, no. 88, pp. 4361-4369, 2015.
[11] R. S. Lee, F. Gimenez, A. Hoogi, K. K. Miyake, M. Gorovoy, and D. L. Rubin, "A curated mammography data set for use in computer-aided detection and diagnosis research," Scientific Data, vol. 4, no. 1, pp. 1-9, 2017

INTERNATIONAL STANDARD SERIAL NUMBER INDIA

INNO SPACE SJIF Scientific Journal Impact Factor

doi crossref

निस्केयर NISCAIR

INTERNATIONAL JOURNAL OF INNOVATIVE RESEARCH

IN COMPUTER & COMMUNICATION ENGINEERING

9940 572 462 6381 907 438 ijircce@gmail.com

www.ijircce.com

Scan to save the contact details